Bull Math Biol manuscript No.
(will be inserted by the editor)

Multiple Scale Homogenisation of Nutrient Movement and Crop Growth in Partially Saturated Soil

Simon J. Duncan · Keith R. Daly · Daniel M. McKay Fletcher · Siul Ruiz · Paul Sweeney · Tiina Roose

Received: / Accepted:

Abstract In this paper, we use multiple scale homogenisation to derive a set of averaged macroscale equations that describe the movement of nutrients in partially saturated soil that contains growing potato tubers. The soil is modelled as a poroelastic material, which is deformed by the growth of the tubers, where the growth of each tuber is dependent on the uptake of nutrients via a sink term within the soil representing root nutrient uptake. Special attention is paid to the reduction in void space, resulting change in local water content and the impact on nutrient diffusion within the soil as the tubers increase in size. To validate the multiple scale homogenisation procedure, we compare the system of homogenised equations to the original set of equations and find that the solutions between the two models differ by $\lesssim 2\%$. However, we find that the computation time between the two sets of equations differs by several orders of magnitude. This is due to the combined effects of the complex

Simon J. Duncan
School of Engineering, Faculty of Engineering and Physical Sciences, University of Southampton, UK, SO17

Keith R. Daly
School of Engineering, Faculty of Engineering and Physical Sciences, University of Southampton, UK, SO17

Daniel M. McKay Fletcher
School of Engineering, Faculty of Engineering and Physical Sciences, University of Southampton, UK, SO17

Siul Ruiz
School of Engineering, Faculty of Engineering and Physical Sciences, University of Southampton, UK, SO17

Paul Sweeney
Syngenta, Jealott's Hill, Bracknell, UK, RG42 6EY.

Tiina Roose
School of Engineering, Faculty of Engineering and Physical Sciences, University of Southampton, UK, SO17
E-mail: T.Roose@soton.ac.uk

three-dimensional geometry and the implementation of a moving boundary condition to capture tuber growth.

Keywords Homogenisation · Deforming geometry · Diffusion · Solute movement

1 Introduction

Application of solutes such as fertilisers and pesticides is important in modern agricultural practices [21]. However, more efficient solute application is needed in order to mitigate growing costs of fertilisers and environmental pollution *i.e.* fertiliser and pesticide buffering, leaching and run off [21]. Hence, understanding water and solute movement in soil is vital for determining sustainable crop production for long-term food security [10]. To aid with this goal, mathematical modelling of soil systems has been studied increasingly in recent years [44], since this offers one method to investigate plant-soil interactions while reducing time and resources compared to standard experimental practices. Combining mathematical modelling with traditional experiments allows us to efficiently improve our understanding of plant-soil interactions [37,11]. This can lead to further improvement of agricultural techniques for greater crop yield while minimising waste of resources.

Mathematical modelling of soil systems covers a wide range of spatial scales, including pore, plant and field scales [14,22]. As such, when studying transport of water and solutes in soil, complex geometries are often required to capture the intrinsic details contained in the microscopic structure of the scale that is considered. This typically requires vast amounts of computation time and resources [12]. Hence, it is often favourable to construct an averaged macroscopic geometry so that the macroscale transport properties can be attained directly from the microscale information [7]. One technique that is frequently used to obtain macroscale movement of fluids and solutes in soil or other porous media is multiple scale homogenization [23]. This mathematical technique is a method of devising a system of averaged macroscopic equations that are parameterised by associated cell problems, which are derived from the inherent microscopic structure of the domain [31].

Multiple scale homogenisation has been successfully used in a wide range of porous media and soil applications including: modelling saturated fluid flow [24], two-phase fluid flow [13], wave propagation in poroelastic materials [40] and single-phase fluid flow in double porosity systems [4]. One application that has been increasingly studied in recent years is homogenisation of moving interfaces for first and second order partial differential equations [8,27]. Although there has been extensive research on the mathematical theory for the homogenisation of moving interfaces, few applications have been explored.

In this study, we demonstrate the utility of homogenisation by modelling the growth of potato tubers in soil, in which the growth is dependent on the quantity of nutrients the plant is able to draw up from the soil. We model the soil as a poroelastic material, such that any growth from a single crop will

influence the water content adjacent to the plant and therefore the movement of nutrients in the vicinity. We use a combination of poroelastic theory and the diffusion equation in porous media to model the movement of nutrients in a deforming soil environment. We develop a series of approximate equations to describe nutrient movement, growth in tuber size and global nutrient uptake in soil.

There has been previous research which studied the effect of diffusion with spatially varying objects in porous media [7], in which Rayleigh's multipole method was used to determine a spatially dependent effective diffusion coefficient based on the size of the sphere within the microscopic periodic geometry [33]. Here we extend this idea to model both spatially and temporally varying objects in poroelastic media, which are coupled to the diffusion of the species within the material itself.

For simplicity we choose to model the tubers as spherical objects in soil, however, this can be extended to any 3D geometry, including, but not limited to, ovoids, capsules and cylinders. To validate the homogenisation procedure, we compare the solution of the homogenised equations against the full system for a series of case studies. This shows the homogenised equations successfully capture the growth of each tuber and the change in nutrient diffusion from the reduction of volume within the domain.

2 Theory

2.1 Three-Phase Poroelastic Soils

Let $\tilde{\mathbf{\Psi}} \subset \mathbb{R}^3$ be an open bounded subset representing a soil system (Figure 1) that contains N potato tubers. We define $\tilde{\mathbf{\Psi}} = \tilde{\mathbf{\Psi}}_{\text{Soil}} \cup \sum_{j=1}^{N} \tilde{\mathbf{\Psi}}_{p_j}$, where $\tilde{\mathbf{\Psi}}_{\text{Soil}}$ is the deformable poroelastic soil domain that is composed of water, air and solid components, and $\tilde{\mathbf{\Psi}}_{p_j}$ are the $j = 1, \ldots, N$ potato tubers each with a boundary $\tilde{\mathbf{\Gamma}}_j$.

To describe the deformable poroelastic soil domain $\tilde{\mathbf{\Psi}}_{\text{Soil}}$, we impose a system of equations that describe a three-phase poroelastic domain. To derive the system of equations, we use the conservation laws for mass and momentum. The conservation of mass equations for the three phases of air, water and soil solid are,

$$\partial_{\tilde{t}} \phi_a = -\tilde{\boldsymbol{\nabla}} \cdot (\phi_a \tilde{\mathbf{v}}_a), \quad \tilde{\mathbf{x}} \in \tilde{\mathbf{\Psi}}_{\text{Soil}}, \tag{1}$$

$$\partial_{\tilde{t}} \phi_w = -\tilde{\boldsymbol{\nabla}} \cdot (\phi_w \tilde{\mathbf{v}}_w) - \lambda_c (\tilde{p}_w - p_r), \quad \tilde{\mathbf{x}} \in \tilde{\mathbf{\Psi}}_{\text{Soil}}, \tag{2}$$

$$\partial_{\tilde{t}} \phi_s = -\tilde{\boldsymbol{\nabla}} \cdot (\phi_s \tilde{\mathbf{v}}_s), \quad \tilde{\mathbf{x}} \in \tilde{\mathbf{\Psi}}_{\text{Soil}}, \tag{3}$$

$$\phi_a + \phi_w + \phi_s = 1, \tag{4}$$

where ϕ_a is the volumetric air content, ϕ_w is the volumetric water content, ϕ_s is the volumetric soil solid content, $\tilde{\mathbf{v}}_a$ is the air velocity, $\tilde{\mathbf{v}}_w$ is the water velocity, $\tilde{\mathbf{v}}_s$ is the velocity of the soil solid component, $\tilde{p}_w$ is the soil water pore pressure. Water uptake in our simulations is assumed to be dominated by transport

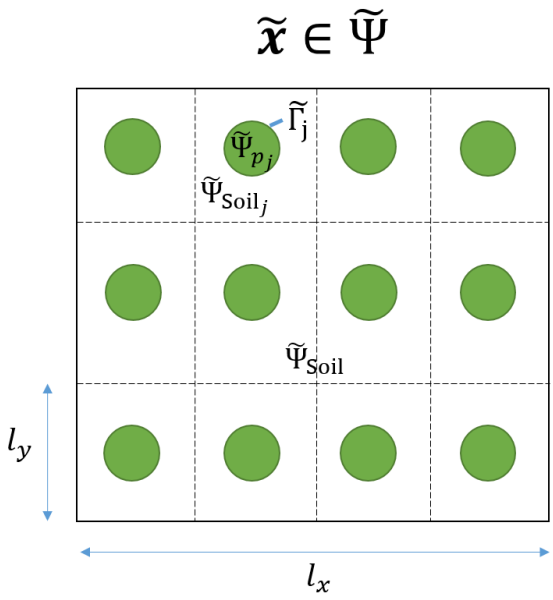

Fig. 1 Schematic of a dimensional poroelastic domain, where $\tilde{\boldsymbol{\Psi}}$ is the total domain, $\tilde{\boldsymbol{\Psi}}_{\mathrm{Soil}}$ is the deformable poroelastic soil domain, $\tilde{\boldsymbol{\Psi}}_{p_j}$ are the potato tubers, $\tilde{\boldsymbol{\Psi}}_{\mathrm{Soil}_j}$ are the poroelastic soil subdomains adjacent to each tuber and $\tilde{\boldsymbol{\Gamma}}_j$ are the boundaries between $\tilde{\boldsymbol{\Psi}}_{p_j}$ and $\tilde{\boldsymbol{\Psi}}_{\mathrm{Soil}}$. In addition, l_x is the macroscale and l_y is the microscale.

through symplastic pathways, thus passively taken up by pressure gradients in the root xylem [35]. The ratio between the cortex and the xylem hydraulic conductivities along with the root surface area density is characterized by λ_c, and the root xylem pressure is expressed as p_r. Roots are assumed to be uniformly distributed throughout the soil domain. We note that we neglect the impact that tuber growth has on the root system. The expression $-\lambda_c(\tilde{p}_w - p_r)$ represents water uptake by plant roots.

Furthermore, Darcy's law for the relative phase velocity of air and water is written as,

$$\phi_a \left(\tilde{\mathbf{v}}_a - \tilde{\mathbf{v}}_s\right) = -\frac{\kappa_a}{\mu_a}\tilde{\boldsymbol{\nabla}}\tilde{p}_a, \quad \tilde{\mathbf{x}} \in \tilde{\boldsymbol{\Psi}}_{\mathrm{Soil}}, \tag{5}$$

$$\phi_w \left(\tilde{\mathbf{v}}_w - \tilde{\mathbf{v}}_s\right) = -\frac{\kappa_w}{\mu_w}\tilde{\boldsymbol{\nabla}}\tilde{p}_w, \quad \tilde{\mathbf{x}} \in \tilde{\boldsymbol{\Psi}}_{\mathrm{Soil}}, \tag{6}$$

where $\tilde{p}_a$ is the soil air pore pressure, κ_a and κ_w are the air and water permeabilities respectively, and μ_a and μ_w are the viscosities of air and water respectively.

The air and water pressures $\tilde{p}_a$ and $\tilde{p}_w$, and the air and water volume fractions ϕ_a and ϕ_w are related via the van Genuchten saturation expression

[42],

$$S_w = \left[\left(\frac{\tilde{p}_a - \tilde{p}_w}{p_c} \right)^{\frac{1}{1-m}} + 1 \right]^{-m}, \tag{7}$$

where $S_w = \phi_w/(\phi_w + \phi_a)$ is the relative water saturation, p_c is the characteristic suction pressure and m is the van Genuchten parameter.

The conservation of momentum equation is [45],

$$\tilde{\boldsymbol{\nabla}} \cdot \mathfrak{G} = 0, \quad \tilde{\mathbf{x}} \in \tilde{\boldsymbol{\Psi}}_{\text{Soil}}, \tag{8}$$

$$\mathfrak{G} = G\left[\left(\tilde{\boldsymbol{\nabla}} \tilde{\mathbf{u}}_s \right) + \left(\tilde{\boldsymbol{\nabla}} \tilde{\mathbf{u}}_s \right)^T + \frac{\nu}{1-2\nu} \tilde{\boldsymbol{\nabla}} \cdot \tilde{\mathbf{u}}_s \mathfrak{T} \right] - S_w \tilde{p}_w \mathfrak{T} - S_a \tilde{p}_a \mathfrak{T}, \tag{9}$$

where $\mathfrak{G}$ is the stress tensor, $\tilde{\mathbf{u}}_s$ is the displacement of the solid soil matrix, G is the shear modulus of the soil solid, ν is the Poisson ratio, $S_a = \phi_a/(\phi_w + \phi_a)$ is the relative air saturation and $\mathfrak{T}$ is the identity tensor. The displacement $\tilde{\mathbf{u}}_s$ is related to $\tilde{\mathbf{v}}_s$ by the relationship,

$$\tilde{\mathbf{v}}_s = \partial_{\tilde{t}} \tilde{\mathbf{u}}_s. \tag{10}$$

The system of equations (1)−(10) completes a full mathematical description of a three-phase poroelastic soil.

2.2 Diffusion of Nutrients in Soil

Solutes such as nutrients typically exist in one of two states in soil, either sorbed to the soil solid surfaces or dissolved in the pore water [36]. We state that the nutrient concentration in the sorbed state follows a reversible linear binding reaction such that,

$$\partial_{\tilde{t}} \tilde{c}_s = d_s, \quad \tilde{\mathbf{x}} \in \tilde{\boldsymbol{\Psi}}_{\text{Soil}}, \tag{11}$$

where $\tilde{c}_s$ is the sorbed nutrient concentration and d_s is the net transfer rate to the sorbed phase from the pore water phase. From conservation of mass, the rate of change of the nutrient concentration in the pore water phase is,

$$\partial_{\tilde{t}}(\phi_w \tilde{c}) = \tilde{\boldsymbol{\nabla}} \cdot \left(D \phi_w \tilde{\boldsymbol{\nabla}} \tilde{c} \right) + d_l - g\tilde{c}, \quad \tilde{\mathbf{x}} \in \tilde{\boldsymbol{\Psi}}_{\text{Soil}}, \tag{12}$$

where $\tilde{c}$ is the nutrient concentration in pore water, d_l is the net transfer rate to the pore water phase from the sorbed phase, D is the diffusion coefficient and g is the nutrient uptake rate from plant roots. Adding (11) and (12) yields,

$$\partial_{\tilde{t}}(\tilde{c}_s + \phi_w \tilde{c}) = \tilde{\boldsymbol{\nabla}} \cdot \left(D \phi_w \tilde{\boldsymbol{\nabla}} \tilde{c} \right) + d_s + d_l - g\tilde{c}, \quad \tilde{\mathbf{x}} \in \tilde{\boldsymbol{\Psi}}_{\text{Soil}}. \tag{13}$$

We assume there is a direct jump between the nutrients in the two states with no intermediate phase, such that $d_s + d_l = 0$. Furthermore, we define d_s,

$$d_s = k_a \tilde{c} - k_d \tilde{c}_s = \partial_{\tilde{t}} \tilde{c}_s, \tag{14}$$

where k_a is the adsorption rate of the nutrient in solution and k_d is the desorption rate. We assume k_d is sufficiently large such that $d_s/k_d = \partial_{\tilde{t}}\tilde{c}_s/k_d \ll 1$ and $k_a \sim k_d$, then,

$$\tilde{c}_s = b\tilde{c}, \tag{15}$$

where $b = k_a/k_d$ is the buffer power of the nutrient [28,6,34]. This leads to the governing equation for nutrient movement in terms of $\tilde{c}$ only, *i.e.*,

$$(\phi_w + b)\partial_{\tilde{t}}\tilde{c} + \tilde{c}\partial_{\tilde{t}}\phi_w = \tilde{\boldsymbol{\nabla}} \cdot \left(D\phi_w \tilde{\boldsymbol{\nabla}}\tilde{c}\right) - g\tilde{c}, \quad \tilde{\mathbf{x}} \in \tilde{\boldsymbol{\Psi}}_{\text{Soil}}. \tag{16}$$

2.3 Boundary Conditions

Here we define a series of boundary conditions on the interfaces $\tilde{\boldsymbol{\Gamma}}_j$, *i.e.*, between the deformable poroelastic soil domain $\tilde{\boldsymbol{\Psi}}_{\text{Soil}}$ and the potato tubers $\tilde{\boldsymbol{\Psi}}_{p_j}$. To describe nutrient interaction on $\tilde{\boldsymbol{\Gamma}}_j$ we impose a zero flux condition, as the potato tubers take up nutrients through their rooting systems and not through the tuber surfaces:

$$\hat{\mathbf{n}} \cdot \left(D\phi_w \tilde{\boldsymbol{\nabla}}\tilde{c}\right) = 0, \quad \tilde{\mathbf{x}} \in \tilde{\boldsymbol{\Gamma}}_j, \tag{17}$$

where $\hat{\mathbf{n}}$ is the unit normal vector pointing out of the geometry. Furthermore, on $\tilde{\boldsymbol{\Gamma}}_j$ we assume the soil solid is displaced normally to the direction of the growing tuber, hence,

$$(2\hat{\mathbf{n}} \otimes \hat{\mathbf{n}} - \mathfrak{T}) \cdot \tilde{\mathbf{u}}_s = \hat{\mathbf{n}}\xi_j, \quad \tilde{\mathbf{x}} \in \tilde{\boldsymbol{\Gamma}}_j, \tag{18}$$

where ξ_j is the displacement of the j^{th} tuber given by,

$$\xi_j = \tilde{r}_j - r^*, \tag{19}$$

where r^* is the initial radius of the tubers and $\tilde{r}_j$ is the radius of the j^{th} tuber, which is related to the total amount of nutrients taken up by the roots. The growth of each tuber is expressed as,

$$\partial_{\tilde{t}}\tilde{V}_j = \alpha \int_{\tilde{\boldsymbol{\Psi}}_{\text{Soil}_j}} g\tilde{c}\; d\tilde{\boldsymbol{\Psi}}_{\text{Soil}_j}, \tag{20}$$

where $\tilde{V}_j$ is the tuber volume, α is the ratio between the rate of growth and uptake, and $\tilde{\boldsymbol{\Psi}}_{\text{Soil}_j}$ is the volume of soil adjacent to each potato tuber j (see Figure 1). Here we model the early-stage development of potato tubers (diameter 5 cm - 7 cm), hence, we approximate the tubers shape to be spherical. Therefore, equation (20) can be written in terms of the radius $\tilde{r}_j$ only, *i.e.*,

$$\partial_{\tilde{t}}\tilde{r}_j = \frac{\alpha}{4\pi\tilde{r}_j^2} \int_{\tilde{\boldsymbol{\Psi}}_{\text{Soil}_j}} g\tilde{c}\; d\tilde{\boldsymbol{\Psi}}_{\text{Soil}_j}. \tag{21}$$

We state the water and air components of $\tilde{\mathbf{\Psi}}_{\text{Soil}}$ do not penetrate the tubers $\tilde{\mathbf{\Psi}}_{p_j}$, thus, we require the Darcy velocities normal to the interface to be zero, *i.e.*,

$$\hat{\mathbf{n}} \cdot \left(\frac{\kappa_w}{\mu_w} \tilde{\boldsymbol{\nabla}} \tilde{p}_w \right) = 0, \quad \tilde{\mathbf{x}} \in \tilde{\mathbf{\Gamma}}_j, \tag{22}$$

$$\hat{\mathbf{n}} \cdot \left(\frac{\kappa_a}{\mu_a} \tilde{\boldsymbol{\nabla}} \tilde{p}_a \right) = 0, \quad \tilde{\mathbf{x}} \in \tilde{\mathbf{\Gamma}}_j. \tag{23}$$

Finally, on $\tilde{\mathbf{\Gamma}}_j$ we assume the the air and water velocities are equal to the growth of the tubers, hence,

$$(2\hat{\mathbf{n}} \otimes \hat{\mathbf{n}} - \mathfrak{T}) \cdot \tilde{\mathbf{v}}_w = \hat{\mathbf{n}} \partial_{\tilde{t}} \tilde{r}_j, \quad \tilde{\mathbf{x}} \in \tilde{\mathbf{\Gamma}}_j, \tag{24}$$

$$(2\hat{\mathbf{n}} \otimes \hat{\mathbf{n}} - \mathfrak{T}) \cdot \tilde{\mathbf{v}}_a = \hat{\mathbf{n}} \partial_{\tilde{t}} \tilde{r}_j, \quad \tilde{\mathbf{x}} \in \tilde{\mathbf{\Gamma}}_j. \tag{25}$$

2.4 Non-Dimensionalisation

To simplify the model and understand the magnitude of influence of each parameter, we non-dimensionalise the system of equations described above. We are interested in the macroscopic properties of the system of equations whilst retaining the influence of the microscopic structure. Hence, we identify there are two different length scales, the 'microscopic' length scale l_y associated with the inner domain tuber geometry, and the macroscopic length scale l_x associated with the full domain transport of water and nutrients. Under these scales, $l_y/l_x = \varepsilon \ll 1$. We choose to non-dimensionalise using the scaling,

$$\tilde{\mathbf{x}} = l_x \mathbf{x}, \ \tilde{t} = \frac{l_x^2}{D} t, \ \tilde{\mathbf{u}}_s = l_y \mathbf{u}_s, \ \tilde{c} = c_{\max} c,$$
$$\tilde{p}_i = G p_i, \ \tilde{\mathbf{v}}_i = \frac{l_y D}{l_x^2} \mathbf{v}_i, \ \tilde{r} = l_y r, \tag{26}$$

where $c_{\max}$ is the maximum concentration of the nutrient applied to $\tilde{\mathbf{\Psi}}_{\text{Soil}}$ and $i = \{w, a\}$. In (26) we use the macroscopic length scale l_x as the spatial scaling to observe that macroscale propeties, the diffusion timescale $\frac{l_x^2}{D}$ for the time scaling and the shear modulus G for the pressure scaling. Shown in Figure 2 is the non-dimensionalised macroscopic domain $\mathbf{\Psi}$ and microscopic domain $\mathbf{\Omega}$. It follows that the air, water, and solid phase continuity equations become:

$$\partial_t \phi_a = -\varepsilon \boldsymbol{\nabla} \cdot (\phi_a \mathbf{v}_a), \quad \mathbf{x} \in \mathbf{\Psi}_{\text{Soil}}, \tag{27}$$

$$\partial_t \phi_w = -\varepsilon \boldsymbol{\nabla} \cdot (\phi_w \mathbf{v}_w) - \overline{\lambda_c}(p_w - \overline{p_r}), \quad \mathbf{x} \in \mathbf{\Psi}_{\text{Soil}}, \tag{28}$$

$$\partial_t (1 - \phi_a - \phi_w) = -\varepsilon \boldsymbol{\nabla} \cdot [(1 - \phi_a - \phi_w) \partial_t \mathbf{u}_s], \quad \mathbf{x} \in \mathbf{\Psi}_{\text{Soil}}, \tag{29}$$

with the constituative poro-elastic mechanical law represented as:

$$\boldsymbol{\nabla}\cdot\Big[(\boldsymbol{\nabla}\mathbf{u}_s)+(\boldsymbol{\nabla}\mathbf{u}_s)^T+\overline{\nu}\boldsymbol{\nabla}\cdot\mathbf{u}_s\mathfrak{T}- \varepsilon^{-1}\left(S_w p_w\mathfrak{T}-S_a p_a\mathfrak{T}\right)\Big]=0,\quad \mathbf{x}\in\boldsymbol{\Psi}_{\text{Soil}},\tag{30}$$

where the force balances and relative movement of the air and water in the mixture domain are represented as:

$$\phi_a\left(\mathbf{v}_a-\partial_t\mathbf{u}_s\right)=-\overline{\kappa}_a\boldsymbol{\nabla}p_a,\quad \mathbf{x}\in\boldsymbol{\Psi}_{\text{Soil}}.\tag{31}$$

$$\phi_w\left(\mathbf{v}_w-\partial_t\mathbf{u}_s\right)=-\overline{\kappa}_w\boldsymbol{\nabla}p_w,\quad \mathbf{x}\in\boldsymbol{\Psi}_{\text{Soil}}.\tag{32}$$

The relationship between water and air are linked based on the Van-Genuchten water retention relationship:

$$S_w=\left\{\left[\overline{G}(p_a-p_w)\right]^{\frac{1}{1-m}}+1\right\}^{-m}.\tag{33}$$

The nutrients in the system follow the convection-diffusion equation:

$$(\phi_w+b)\partial_t c+c\partial_t\phi_w=\boldsymbol{\nabla}\cdot(\phi_w\boldsymbol{\nabla}c)-\overline{g}c,\quad \mathbf{x}\in\boldsymbol{\Psi}_{\text{Soil}},\tag{34}$$

where we have no flux through the tuber surface:

$$\hat{\mathbf{n}}\cdot(\phi_w\boldsymbol{\nabla}c)=0,\quad \mathbf{x}\in\boldsymbol{\Gamma}_j.\tag{35}$$

The soil solid phase displacement is equal to the increase in the tuber radius:

$$(2\hat{\mathbf{n}}\otimes\hat{\mathbf{n}}-\mathfrak{T})\cdot\mathbf{u}_s=\hat{\mathbf{n}}(r_j-\overline{r^*}),\quad \mathbf{x}\in\boldsymbol{\Gamma}_j.\tag{36}$$

Neither water nor air are assumed to flow through the tuber surface:

$$\hat{\mathbf{n}}\cdot(\boldsymbol{\nabla}p_w)=0,\quad \mathbf{x}\in\boldsymbol{\Gamma}_j,\tag{37}$$

$$\hat{\mathbf{n}}\cdot(\boldsymbol{\nabla}p_a)=0,\quad \mathbf{x}\in\boldsymbol{\Gamma}_j.\tag{38}$$

The water and air velocities normal to the tuber surface also follow the rate of the tuber growth:

$$(2\hat{\mathbf{n}}\otimes\hat{\mathbf{n}}-\mathfrak{T})\cdot\mathbf{v}_w=\hat{\mathbf{n}}\partial_t r_j,\quad \mathbf{x}\in\boldsymbol{\Gamma}_j,\tag{39}$$

$$(2\hat{\mathbf{n}}\otimes\hat{\mathbf{n}}-\mathfrak{T})\cdot\mathbf{v}_a=\hat{\mathbf{n}}\partial_t r_j,\quad \mathbf{x}\in\boldsymbol{\Gamma}_j.\tag{40}$$

Finally, the tuber growth rate is based on the rate of nutrient uptake out of the system:

$$\partial_t r_j=\frac{\overline{\alpha}}{4\pi r_j^2}\int_{\boldsymbol{\Psi}_{\text{Soil}_j}} c\; d\boldsymbol{\Psi}_{\text{Soil}_j}.\tag{41}$$

Here the system was non-dimensionalised as follows:

$$\overline{\lambda_c}=\frac{\lambda_c G l_x^2}{D},\ \overline{p_r}=\frac{p_r}{G},\ \overline{\nu}=\frac{\nu}{1-2\nu},\ \overline{\kappa}_a=\frac{\kappa_a G\varepsilon^{-1}}{D\mu_a},\ \overline{\kappa}_w=\frac{\kappa_w G\varepsilon^{-1}}{D\mu_w},$$
$$\overline{G}=\frac{G}{p_c},\ \overline{g}=\frac{g l_x^2}{D},\overline{r^*}=\frac{r^*}{l_y},\overline{\alpha}=\frac{c_{\max}\alpha g l_x^2}{D}.\tag{42}$$

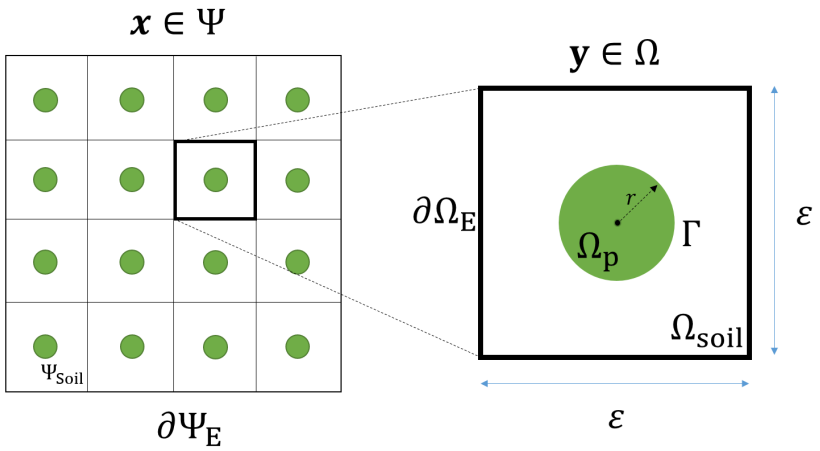

Fig. 2 Schematic of the dimensionless macroscale domain $\boldsymbol{\Psi}$ and microscale domain $\boldsymbol{\Omega}$, where $\boldsymbol{\Psi}_{\text{Soil}}$ is the poroelastic soil domain, $\partial\boldsymbol{\Psi}_E$ is the external boundary of $\boldsymbol{\Psi}$, $\boldsymbol{\Omega}_{\text{Soil}}$ is the poroelastic domain composed of water, air and solid components, $\boldsymbol{\Omega}_p$ is the potato tuber, $\boldsymbol{\Gamma}$ is the boundary between $\boldsymbol{\Omega}_{\text{Soil}}$ and $\boldsymbol{\Omega}_p$, $\partial\boldsymbol{\Omega}_E$ is the external boundary of the periodic cell and r is the radius of $\boldsymbol{\Omega}_p$.

2.5 Parameter Estimation

Here we estimate the parameters contained in equations (27)−(41) in order to determine the magnitude of influence each parameter has on the system of equations. Since this model is motivated by the growth of potato tubers in soil, we assess the parameter values for silt soils as potatoes are frequently grown in this soil type [41].

Potato plants are typically grown in ridge and furrow type systems and are contained in the plough layer of soil, which is the top 30 cm of soil [26]. Hence, we choose the macroscopic length scale to be $l_x \approx 0.3$ m. Similarly, we assume that the tubers have an inter-tuber distance that is substantially less than the total length of the plough layer. We choose an inter-tuber distance of approximately $l_y \approx 0.05$ m, resulting in the ratio of the two length scales to be $\varepsilon \approx 0.1$. We also assume an initial tuber radius of $r^* = \mathcal{O}(0.05)$ m $< l_y$.

Values for the Poisson ratio of silt soils are approximately $0.3 \lesssim \nu \lesssim 0.35$ [18], and the shear modulus is $G \approx 1 \times 10^7$ Pa [43]. Furthermore, typical characteristic suction pressures for silt soils are approximately $p_c \approx 3 \times 10^4$ Pa [42], with soil permeabilities of $\kappa_w \approx \kappa_a \approx 5 \times 10^{-14}$ m^2 [42]. The viscosity of water is $\mu_w \approx 10^{-3}$ Pa s and the viscosity of air is $\mu_a \approx 10^{-5}$ Pa s.

One of the key nutrients responsible for plant growth and development is nitrogen [28]. We choose to model this nutrient since plant growth is closely linked to abundance of nitrogen in soil. Nitrogen has a diffusion coefficient

in soil water of $D \approx 2.5 \times 10^{-10}$ m^2 s^{-1} [6]. Furthermore, for the potato plant *Solanum tuberosum* L, the uptake rate of the nutrient nitrogen is $g \approx 1 \times 10^{-9}$ s^{-1} [39,5]. This was found to be in nitrogen concentrations in soil of $c_{\max} \approx 10^{-1}$kg m^{-3} [5].

In early-stage growth of *Solanum tuberosum* L plants, the tuber radius growth rate is approximately 1×10^{-9} m s^{-1} [46]. If we assume that the quantity of nitrogen that is taken up by the plant is proportional to the growth of the tuber, then we can estimate the ratio between the rate of growth and the uptake, *i.e.*, $\alpha \approx 1 \times 10^{1}$ kg^{-1} m^{-1} [39,5].

Using the values above, we find that the parameters $\overline{\kappa}_a$ and $\overline{\kappa}_w$ in equations (31) and (32) are $\overline{\kappa}_a = \mathcal{O}(10^9)$ and $\overline{\kappa}_w = \mathcal{O}(10^7)$. This is significantly larger than the other terms in the equations. Hence, we re-write equations (31) and (32) so that,

$$\boldsymbol{\nabla} p_a \approx 0, \quad \mathbf{x} \in \boldsymbol{\Psi}_{\text{Soil}}, \tag{43}$$

$$\boldsymbol{\nabla} p_w \approx 0, \quad \mathbf{x} \in \boldsymbol{\Psi}_{\text{Soil}}, \tag{44}$$

which have the solutions p_a = constant and p_w = constant, *i.e.*, the consolidation of the soil is substantially faster than the diffusion of solutes. Since p_w = constant, we find that the sink term in equation (2) representing root uptake is constant, *i.e.*, $\lambda_c(\tilde{p}_w - p_r) = F$, where F is the water uptake rate by plant roots. The uptake rate of water from *Solanum tuberosum*, L roots is $F \approx 1 \times 10^{-8}$ s^{-1} [30].

From equation (33), the solutions p_a = constant and p_w = constant result in S_w = constant, and since $S_w + S_a = 1$, this leads to S_a = constant. Although S_w is constant, ϕ_w will still change as a function of the changing domain geometry. Substituting 44 into 32 renders the domain water content to become dependent on the solid phase displacements:

$$\partial_t \mathbf{u}_s = \mathbf{v}_w, \quad \mathbf{x} \in \boldsymbol{\Psi}_{\text{Soil}}. \tag{45}$$

Thus, we reduce the system of equations (27)−(41) to,

$$\partial_t \phi_w = -\varepsilon \boldsymbol{\nabla} \cdot (\phi_w \partial_t \mathbf{u}_s) - \overline{F}, \quad \mathbf{x} \in \boldsymbol{\Psi}_{\text{Soil}}, \tag{46}$$

$$\boldsymbol{\nabla} \cdot \left[(\boldsymbol{\nabla} \mathbf{u}_s) + (\boldsymbol{\nabla} \mathbf{u}_s)^T + \overline{\nu} \boldsymbol{\nabla} \cdot \mathbf{u}_s \mathfrak{T} \right] = 0, \quad \mathbf{x} \in \boldsymbol{\Psi}_{\text{Soil}}, \tag{47}$$

$$(\phi_w + b)\partial_t c + c \partial_t \phi_w = \boldsymbol{\nabla} \cdot (\phi_w \boldsymbol{\nabla} c) - \overline{g} c, \quad \mathbf{x} \in \boldsymbol{\Psi}_{\text{Soil}}, \tag{48}$$

$$(2\hat{\mathbf{n}} \otimes \hat{\mathbf{n}} - \mathfrak{T}) \cdot \mathbf{u}_s = \hat{\mathbf{n}}(r_j - \overline{r^*}), \quad \mathbf{x} \in \boldsymbol{\Gamma}_j, \tag{49}$$

$$\hat{\mathbf{n}} \cdot (\phi_w \boldsymbol{\nabla} c) = 0, \quad \mathbf{x} \in \boldsymbol{\Gamma}_j, \tag{50}$$

$$\partial_t r_j = \frac{\overline{\alpha}}{4\pi r_j^2} \int_{\boldsymbol{\Psi}_{\text{Soil}_j}} c \, d\boldsymbol{\Psi}_{\text{Soil}_j}, \tag{51}$$

where $\overline{F} = F l_x^2 / D$.

Using the values discussed above, we find that the parameters contained in (46)−(51) have the approximate values,

$$\overline{F} = \mathcal{O}(1), \ \overline{\nu} = \mathcal{O}(1), \ \overline{g} = \mathcal{O}(1), \overline{r^*} = \mathcal{O}(1), \overline{\alpha} = \mathcal{O}(1). \tag{52}$$

For the remainder of this study, equations (46)−(51) will be referred to as the 'full set' of equations to describe solute movement and tuber growth.

2.6 Homogenisation

In this section, we use multiple scale homogenisation to develop a set of averaged macroscale equations that describe the movement of nutrients and tuber growth in soil. From equation (46) we observe that ϕ_w is affected by two mechanisms: firstly by soil compression due to the growth of the tuber, *i.e.*, $\varepsilon\boldsymbol{\nabla}\cdot(\phi_w\mathbf{v}_s)$, and secondly by root water uptake, *i.e.*, $\overline{F}$. From the non-dimensionalisation, we observe that the maximum displacement is bounded such that $\mathbf{u}_s \ll \overline{F}$. This leads to the results $\partial_t\mathbf{u}_s \ll \overline{F}$. If we consider a scenario when the tubers are not taking up water, eq. 45 suggests that the primary change in water content is based on $\varepsilon\boldsymbol{\nabla}\cdot(\phi_w\partial_t\mathbf{u}_s)$. Since $\varepsilon\boldsymbol{\nabla}\cdot(\phi_w\partial_t\mathbf{u}_s) \ll \partial_t\mathbf{u}_s$ and $\partial_t\mathbf{u}_s \ll \overline{F}$, then it follows that $\varepsilon\boldsymbol{\nabla}\cdot(\phi_w\partial_t\mathbf{u}_s) \ll \overline{F}$. Therefore, we find that the root water uptake term dominates the change in water content. Hence, for the homogenisation procedure, we neglect the term regarding soil compression, and the system of equations we homogenise reduces to,

$$\partial_t\phi_w = -\overline{F}, \quad \mathbf{y}\in\boldsymbol{\Omega}_{\text{Soil}}, \tag{53}$$

$$(\phi_w + b)\partial_t c + c\partial_t\phi_w = \boldsymbol{\nabla}\cdot(\phi_w\boldsymbol{\nabla}c) - \overline{g}c, \quad \mathbf{y}\in\boldsymbol{\Omega}_{\text{Soil}}, \tag{54}$$

$$\hat{\mathbf{n}}\cdot(\phi_w\boldsymbol{\nabla}c) = 0, \quad \mathbf{y}\in\boldsymbol{\Gamma}, \tag{55}$$

$$\partial_t r = \frac{\overline{\alpha}}{4\pi r^2}\int_{\boldsymbol{\Omega}_{\text{Soil}}} c\; d\boldsymbol{\Omega}_{\text{Soil}}. \tag{56}$$

$$\text{periodic } \mathbf{y}\in\partial\boldsymbol{\Omega}_E. \tag{57}$$

To validate this assumption, we compare the full set of equations (46)−(51) to the homogenised system of equations derived from (53)−(57) in the following section. We highlight that the horizontal boundaries for the full model preserve the periodicity presented here.

We observe there are two different length scales present in the geometry $\tilde{\boldsymbol{\Psi}}$, the macroscale l_x and the mircoscale l_y. Any change of $\mathcal{O}(1)$ on the length scale l_x will result in a $\mathcal{O}(\varepsilon)$ change on the length scale l_y. We can formalise this by assuming that the dependent variables ϕ_w, c and r are functions of a small scale $\mathbf{y}$ and a large scale $\mathbf{x}$. We denote the unit cell $\boldsymbol{\Omega}$ representing the microscale domain $\mathbf{y}\in\boldsymbol{\Omega}\equiv[-1/2,1/2]^3$. Using the two length scales and chain rule, the gradient operator is written as,

$$\boldsymbol{\nabla} = \boldsymbol{\nabla}_{\mathbf{x}} + \varepsilon^{-1}\boldsymbol{\nabla}_{\mathbf{y}}. \tag{58}$$

Furthermore, we expand ϕ_w, c and r such that,

$$\phi_w = \phi_{w_0} + \mathcal{O}(\varepsilon), \tag{59}$$

$$c = c_0 + \varepsilon c_1 + \varepsilon^2 c_2 + \mathcal{O}(\varepsilon^3), \tag{60}$$

$$r = r_0 + \mathcal{O}(\varepsilon). \tag{61}$$

The first step of the homogenisation procedure is to determine the most dominant terms in the system of equations (53)−(57). To do this we substitute

equations (59)−(61) into (53)−(57) and collecting the largest terms $\mathcal{O}(\varepsilon^{-2})$. This results in the system of equations,

$$\boldsymbol{\nabla}_{\mathbf{y}} \cdot (\phi_{w_0} \boldsymbol{\nabla}_{\mathbf{y}} c_0) = 0, \quad \mathbf{y} \in \boldsymbol{\Omega}_{\text{Soil}}, \tag{62}$$

$$\hat{\mathbf{n}} \cdot (\phi_{w_0} \boldsymbol{\nabla}_{\mathbf{y}} c_0) = 0, \quad \mathbf{y} \in \boldsymbol{\Gamma}, \tag{63}$$

$$\text{periodic } \mathbf{y} \in \partial \boldsymbol{\Omega}_E. \tag{64}$$

Theorem Equations (62)−(64) have the solution $c_0 = c_0(\mathbf{x}, t)$, *i.e.*, c_0 has large scale dependence only.

Proof We observe from (62) that,

$$\int_{\boldsymbol{\Omega}_{\text{Soil}}} c_0 \boldsymbol{\nabla}_{\mathbf{y}} \cdot (\phi_{w_0} \boldsymbol{\nabla}_{\mathbf{y}} c_0) \, d\boldsymbol{\Omega}_{\text{Soil}} = 0. \tag{65}$$

Applying Green's first identity to (65) yields,

$$\int_{\partial \boldsymbol{\Gamma}} c_0 \hat{\mathbf{n}} \cdot (\phi_{w_0} \boldsymbol{\nabla}_{\mathbf{y}} c_0) \, d\boldsymbol{\Gamma} + \int_{\partial \boldsymbol{\Omega}_E} c_0 \hat{\mathbf{n}} \cdot (\phi_{w_0} \boldsymbol{\nabla}_{\mathbf{y}} c_0) \, d\partial\boldsymbol{\Omega}_E - \int_{\boldsymbol{\Omega}_{\text{Soil}}} \boldsymbol{\nabla}_{\mathbf{y}} c_0 \cdot (\phi_{w_0} \boldsymbol{\nabla}_{\mathbf{y}} c_0) \, d\boldsymbol{\Omega}_{\text{Soil}} = 0. \tag{66}$$

Using (63) and (64), we find,

$$\int_{\boldsymbol{\Omega}_{\text{Soil}}} \boldsymbol{\nabla}_{\mathbf{y}} c_0 \cdot (\phi_{w_0} \boldsymbol{\nabla}_{\mathbf{y}} c_0) \, d\boldsymbol{\Omega}_{\text{Soil}} = 0. \tag{67}$$

Equation (67) can be expressed as,

$$\int_{\boldsymbol{\Omega}_{\text{Soil}}} \phi_{w_0} ||\boldsymbol{\nabla}_{\mathbf{y}} c_0||_2^2 \, d\boldsymbol{\Omega}_{\text{Soil}} = 0, \tag{68}$$

where $||\cdot||_2$ is the Euclidean norm, *i.e.*, $||\mathbf{x}||_2 = \sqrt{\langle \mathbf{x}, \mathbf{x} \rangle} = \sqrt{x_1^2 + ... + x_n^2}$. In order to satisfy (68), $||\boldsymbol{\nabla}_{\mathbf{y}} c_0||_2^2 = 0$. By definition, $||\mathbf{x}||_2 = 0 \iff \mathbf{x} = 0$, hence,

$$||\boldsymbol{\nabla}_{\mathbf{y}} c_0||_2^2 = 0 \quad \Rightarrow \quad \boldsymbol{\nabla}_{\mathbf{y}} c_0 = 0 \quad \Rightarrow \quad c_0 = C, \tag{69}$$

where C is an arbitrary constant. Therefore $c_0 = c_0(\mathbf{x}, t)$. □

From the theorem above we observe that c_0 has large scale dependence only and is independent of the small scale $\mathbf{y}$, however, we recieve no other information regarding the solution of c_0.

To proceed with the homogenisation methodology, we collect the next most dominant terms in the system of equations. This is achieved by collecting terms $\mathcal{O}(\varepsilon^{-1})$ and using the results $\boldsymbol{\nabla}_{\mathbf{y}} c_0 = 0$, *i.e.*,

$$\boldsymbol{\nabla}_{\mathbf{y}} \cdot (\phi_{w_0} \boldsymbol{\nabla}_{\mathbf{y}} c_1 + \phi_{w_0} \boldsymbol{\nabla}_{\mathbf{x}} c_0) = 0, \quad \mathbf{y} \in \boldsymbol{\Omega}_{\text{Soil}}, \tag{70}$$

$$\hat{\mathbf{n}} \cdot (\phi_{w_0} \boldsymbol{\nabla}_{\mathbf{y}} c_1 + \phi_{w_0} \boldsymbol{\nabla}_{\mathbf{x}} c_0) = 0, \quad \mathbf{y} \in \boldsymbol{\Gamma}, \tag{71}$$

$$\text{periodic } \mathbf{y} \in \partial\mathbf{\Omega}_E. \tag{72}$$

To ensure (70)−(72) form a well-posed problem, *i.e.*, the equations have a solution that agrees with the boundary conditions, we check the solvability of the system. We can show the system is well-posed by applying the divergence theorem to equation (70) and use the boundary condition (71) such that,

$$\int_{\mathbf{\Omega}_{\text{Soil}}} \boldsymbol{\nabla}_{\mathbf{y}} \cdot (\phi_{w_0} \boldsymbol{\nabla}_{\mathbf{y}} c_1 + \phi_{w_0} \boldsymbol{\nabla}_{\mathbf{x}} c_0)\, d\mathbf{\Omega}_{\text{Soil}} = \int_{\partial\mathbf{\Omega}_{\text{Soil}}} \hat{\mathbf{n}} \cdot (\phi_{w_0} \boldsymbol{\nabla}_{\mathbf{y}} c_1 + \phi_{w_0} \boldsymbol{\nabla}_{\mathbf{x}} c_0)\, d\partial\mathbf{\Omega}_{\text{Soil}} = 0. \tag{73}$$

Next we choose to rescale c_1 such that,

$$c_1(\mathbf{x}, \mathbf{y}) = \sum_{k=1}^{3} \chi_k(\mathbf{y}) \partial_{x_k} c_0 + \bar{c_1}(\mathbf{x}), \tag{74}$$

where $\bar{c_1}(\mathbf{x})$ is the large scale component of $c_1(\mathbf{x}, \mathbf{y})$. Substituting (74) into (70)−(72) yields the cell problem for χ_k,

$$\boldsymbol{\nabla}_{\mathbf{y}} \cdot (\boldsymbol{\nabla}_{\mathbf{y}} \chi_k + \hat{\mathbf{e}}_k) = 0, \quad \mathbf{y} \in \mathbf{\Omega}_{\text{Soil}}, \tag{75}$$

$$\hat{\mathbf{n}} \cdot (\boldsymbol{\nabla}_{\mathbf{y}} \chi_k + \hat{\mathbf{e}}_k) = 0, \quad \mathbf{y} \in \mathbf{\Gamma}, \tag{76}$$

$$\text{periodic } \mathbf{y} \in \partial\mathbf{\Omega}_E, \tag{77}$$

where $\hat{\mathbf{e}}_k$ is the unit vector.

We note that the tubers grow in the soil domain, hence, the cell problem solution χ_k is dependent on the radius of the tuber. Since the cell problem is a representation of the impedance of nutrient movement due to tuber obstruction, and as the tuber grows the impact on nutrient transport will change, therefore we have the relationship $\chi_k = \chi_k(r)$, *i.e.*, the cell problem solution is dependent on the radius of the tuber.

The last step of the homogenisation procedure is to collect terms $\mathcal{O}(\varepsilon^0)$, *i.e.*,

$$\partial_t \phi_{w_0} = -\overline{F}, \quad \mathbf{y} \in \mathbf{\Omega}_{\text{Soil}}, \tag{78}$$

$$(\phi_{w_0} + b)\partial_t c_0 + c_0 \partial_t \phi_{w_0} = \boldsymbol{\nabla}_{\mathbf{y}} \cdot (\phi_{w_0} \boldsymbol{\nabla}_{\mathbf{y}} c_2 + \phi_{w_0} \boldsymbol{\nabla}_{\mathbf{x}} c_1) + \boldsymbol{\nabla}_{\mathbf{x}} \cdot (\phi_{w_0} \boldsymbol{\nabla}_{\mathbf{y}} c_1 + \phi_{w_0} \boldsymbol{\nabla}_{\mathbf{x}} c_0) - \overline{g} c, \quad \mathbf{y} \in \mathbf{\Omega}_{\text{Soil}}, \tag{79}$$

$$\hat{\mathbf{n}} \cdot (\phi_{w_0} \boldsymbol{\nabla}_{\mathbf{y}} c_2 + \phi_{w_0} \boldsymbol{\nabla}_{\mathbf{x}} c_1) = 0, \quad \mathbf{y} \in \mathbf{\Gamma}, \tag{80}$$

$$\text{periodic } \mathbf{y} \in \partial\mathbf{\Omega}_E, \tag{81}$$

$$\partial_t r_0 = \frac{\overline{\alpha}}{4\pi r_0^2} \int_{\mathbf{\Omega}_S} c_0 \, d\mathbf{\Omega}_S. \tag{82}$$

To check (78)−(82) provide a well-posed problem, we check the solvability of the system of equations. To do this, we apply the divergence theorem to (79),

$$\int_{\mathbf{\Omega}_{\text{Soil}}} (\phi_{w_0}+b)\partial_t c_0+c_0\partial_t\phi_{w_0}\ d\mathbf{\Omega}_{\text{Soil}} = \int_{\mathbf{\Omega}_{\text{Soil}}} \boldsymbol{\nabla}_{\mathbf{y}}\cdot(\phi_{w_0}\boldsymbol{\nabla}_{\mathbf{y}}c_2+\phi_{w_0}\boldsymbol{\nabla}_{\mathbf{x}}c_1)\ d\mathbf{\Omega}_{\text{Soil}} + \int_{\mathbf{\Omega}_{\text{Soil}}} \boldsymbol{\nabla}_{\mathbf{x}}\cdot(\phi_{w_0}\boldsymbol{\nabla}_{\mathbf{y}}c_1+\phi_{w_0}\boldsymbol{\nabla}_{\mathbf{x}}c_0)\ d\mathbf{\Omega}_{\text{Soil}} - \int_{\mathbf{\Omega}_{\text{Soil}}} \overline{g}c\ d\mathbf{\Omega}_{\text{Soil}}, \quad (83)$$

and using boundary condition (80) yields,

$$\int_{\mathbf{\Omega}_{\text{Soil}}} (\phi_{w_0}+b)\partial_t c_0+c_0\partial_t\phi_{w_0}\ d\mathbf{\Omega}_{\text{Soil}} = \int_{\mathbf{\Omega}_{\text{Soil}}} \boldsymbol{\nabla}_{\mathbf{x}}\cdot(\phi_{w_0}\boldsymbol{\nabla}_{\mathbf{y}}c_1+\phi_{w_0}\boldsymbol{\nabla}_{\mathbf{x}}c_0)\ d\mathbf{\Omega}_{\text{Soil}} - \int_{\mathbf{\Omega}_{\text{Soil}}} \overline{g}c\ d\mathbf{\Omega}_{\text{Soil}}. \quad (84)$$

We define,

$$||\mathbf{\Omega}_{\text{Soil}}|| = ||\mathbf{\Omega}_{\text{Soil}}(r)|| = \int_{\mathbf{\Omega}_{\text{Soil}}} d\mathbf{\Omega}_{\text{Soil}}, \quad (85)$$

to be the volume integral of the cell problem, which is dependent on the radius of the tuber. It follows that (84) can be written,

$$||\mathbf{\Omega}_{\text{Soil}}||\left[(\phi_{w_0}+b)\partial_t c_0 + c_0\partial_t\phi_{w_0}\right] = \frac{\partial}{\partial x_i}\int_{\mathbf{\Omega}_{\text{Soil}}} \left[\phi_{w_0}\left(\frac{\partial c_0}{\partial x_i}+\frac{\partial \chi_j}{\partial y_i}\frac{\partial c_0}{\partial x_j}\right)\right] d\mathbf{\Omega}_{\text{Soil}} - ||\mathbf{\Omega}_{\text{Soil}}||\overline{g}c_0, \quad \mathbf{y}\in\mathbf{\Omega}_{\text{Soil}}. \quad (86)$$

This results in the approximate equations for ϕ_{w_0}, c_0 and r_0,

$$\partial_t\phi_{w_0} = -\overline{F}, \quad \mathbf{y}\in\mathbf{\Omega}_{\text{Soil}}, \quad (87)$$

$$||\mathbf{\Omega}_{\text{Soil}}(r_0)||\left[(\phi_{w_0}+b)\partial_t c_0 + c_0\partial_t\phi_{w_0}\right] = \phi_{w_0}\boldsymbol{\nabla}_{\mathbf{x}}\cdot(\mathfrak{D}_{\mathfrak{e}}(r_0)\boldsymbol{\nabla}_{\mathbf{x}}c_0) - ||\mathbf{\Omega}_{\text{Soil}}(r_0)||\overline{g}c_0, \quad \mathbf{y}\in\mathbf{\Omega}_{\text{Soil}}, \quad (88)$$

$$\partial_t r_0 = \frac{\overline{\alpha}}{4\pi r_0^2}||\mathbf{\Omega}_{\text{Soil}}(r_0)||c_0, \quad (89)$$

where,

$$\mathfrak{D}_{\mathfrak{e}}(r_0) = \int_{\mathbf{\Omega}_{\text{Soil}}} \mathfrak{T} + \boldsymbol{\nabla}_{\mathbf{y}}\chi_k(r_0)\otimes\hat{\mathbf{e}}_k\ d\mathbf{\Omega}_{\text{Soil}}, \quad (90)$$

for $k=(1,...,3)$.

Here the averaged terms $||\mathbf{\Omega}_{\text{Soil}}(r_0)||$ and $\mathfrak{D}_{\mathfrak{e}}(r_0)$ are parameterised from the cell problem (75)−(77). This result identifies that equations (78)−(82) provide a well-posed problem if and only if the system of equations (87)−(90) have a solution. For the remainder of this study, equations (87)−(90) will be referred to as the 'homogenised set' of equations to describe solute movement and tuber growth.

3 Validation of the Homogenisation Procedure

We validate the mathematical steps used in the homogenisation procedure by comparing the homogenised set of equations (87)−(90) to the full set of equations (46)−(51). We consider multiple comparisons by varying parameters for the buffer power b, root uptake rate $\overline{F}$ and initial volumetric water content $\phi_w|_{t=0}$ to examine the accuracy of the averaging procedure.

We generate two geometries, one for the full set of equations (46)−(51) containing potato tubers, and a second uniform geometry for the homogenised equations (87)−(90). We choose the domain length of each geometry to be composed of eight periodic cells. Due to the homogenisation procedure, the approximate equations (87)−(90) do not require any tubers as the influence of the microscale geometry is contained in the paramterised terms $||\mathbf{\Omega}_{\text{Soil}}(r_0)||$ and $\mathfrak{D}_{\mathfrak{e}}(r_0)$. Shown in Figure 3 are the geometries used to validate the homogenisation procedure.

Lastly, we numerically illustrate that the full solution tends towards the homogenised solution as $\varepsilon \to 0$. Since $\varepsilon = \frac{l_y}{l_x}$, then it suffices to show that the solutions become closer as $l_x \to \infty$, as this implies that $\varepsilon \to 0$. We begin with by setting $l_x = 0.3$, where the domain of the full solution can only consist of 3 tubers. We incrementally increase the domain size up to $l_x = 0.8$, where the domain consists of 8 tubers. We take the percent difference between the homogenised solution for the concentration profile as:

$$d_p = \frac{\|c^{(\varepsilon)} - c_0^{(\varepsilon)}\|_\infty}{\|c^{(\varepsilon)}\|_\infty} \times 100\%, \quad \mathbf{x} \in \mathbf{\Omega}_{\text{Soil}}, \tag{91}$$

where $c^{(\varepsilon)}$ is the solute concentration profile in the full solution as a function of a given epsilon, $c_0^{(\varepsilon)}$ is the solute concentration profile based on the homogenised solution, $\|c^{(\varepsilon)} - c_0^{(\varepsilon)}\|_\infty$is the largest difference between the two solutions for all time points in the whole domain for a fixed ε value, and $\|c^{(\varepsilon)}\|_\infty$ is the supremum concentration value for all time in the full domain for the full solution for a fixed ε value.

To solve the systems of equations, we use the finite element package COMSOL Multiphysics® 5.3 (www.comsol.com). We run our full model with a mesh consisting of 21729 tetrahedral elements and 1405 for the homogenised model. Simulations were run using the MUMPS (Multifrontal Massively Parallel Sparse) direct solver for a fully coupled physical system. In this section, we describe the implementation of each set of equations, and show a comparison between them.

3.1 Full Equations

Implementation of the full set of equations (46)−(51) requires the implementation of a complex moving boundary problem. This accounts for the uptake of nutrients by each tuber $\mathbf{\Psi}_{p_j}$, the subsequent growth of $\mathbf{\Psi}_{p_j}$, and the reduction in volumetric water content ϕ_w. The geometry we impose the full set of

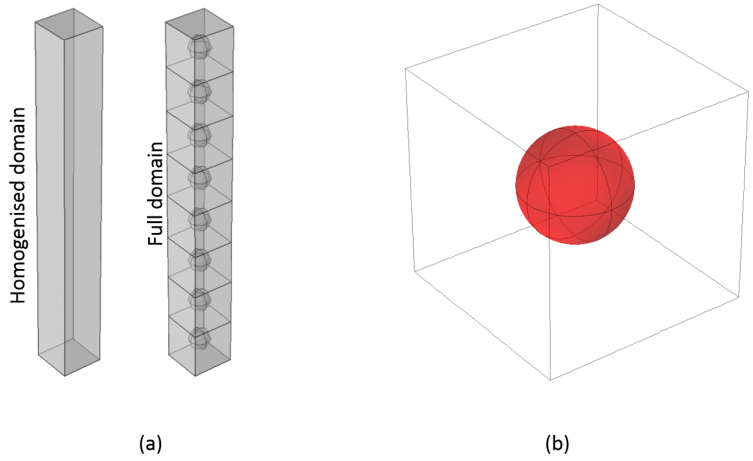

Fig. 3 The geometries used to validate the homogenisation procedure (a): The approximate equations (87)−(90) are solved on the left geometry, whereas the original set of equations (46)−(51) are solved on the right geometry that contains potato tubers. (b): The cell problem is solved on a single unit cell that contains a potato tuber (coloured in red). Comparisons between the homogenised model and the full model were done by analysing the concentrations along the of the domain running down the vertical axes.

equations on can be seen in Figure 3a. However, we require two versions of this geometry; an undeformed geometry that is constant in time, and a deforming geometry that is dependent on tuber growth, since different components of the system (46)−(51) are solved on either an undeformed or deforming frame of reference. There are three main components that are required to be implemented in order to solve (46)−(51), these are: the poroelastic equations, the compaction and deformation of soil, and the nutrient movement equations.

To implement the poroelastic equations (46)−(47) and (49) for the local displacement $\mathbf{u}^s$ and reduction in ϕ_w is straightforward, since these equations are solved on the undeformed geometry regardless of tuber size. Using this solution at each time step, we can prescribe a deformation (for the deforming geometry) within the soil domain to correspond with the increase in tuber size.

The nutrient equations (48) and (50)−(51) are solved on the deforming geometry to correspond with the growth of the tubers. However, these equations use the poroelastic solution from the undeformed geometry. Hence, we implement a reference frame change such that poroelastic solution can be mapped from the undeformed geometry to the deformed geometry. This allows us to

393 solve the nutrient equations on the deformed geometry corresponding with the
394 prescribed tuber deformation.

395 Since the nutrient equations are solved on a deforming geometry, we are re-
396 quired to ensure that c is conserved. This is achieved by making two alterations
397 to (48) and (50). Firstly, we note Reynolds Transport Theorem,

$$\frac{d}{dt}\int_{\theta(t)} \mathbf{F}\ dV = \int_{\theta(t)} \frac{\partial \mathbf{F}}{\partial t}\ dV + \int_{\partial\theta(t)} (\boldsymbol{\omega}\cdot\hat{\mathbf{n}})\mathbf{F}\ dA, \tag{92}$$

398 where, dV and dA are volume and surface elements respectively, $\boldsymbol{\omega}$ is the veloc-
399 ity of the surface element, $\hat{\mathbf{n}}$ is the normal vector pointing out of the geometry,
400 $\mathbf{F}$ is any function of $\mathbf{x}$ and t, and $\theta(t)$ is the domain. Reynolds Transport The-
401 orem states that the change in nutrient concentration in a domain is equal to
402 the change in concentration within the domain plus the rate at which nutrient
403 is entering the domain. Applying equation (92) to the full set of equations we
404 have leads to,

$$\frac{d}{dt}\int_{\boldsymbol{\Psi}_{\mathrm{Soil}(t)}} c\ d\boldsymbol{\Psi}_{\mathrm{Soil}(t)} = \int_{\boldsymbol{\Psi}_{\mathrm{Soil}(t)}} \frac{\partial c}{\partial t}\ d\boldsymbol{\Psi}_{\mathrm{Soil}(t)} + \int_{\partial\boldsymbol{\Psi}_{\mathrm{Soil}(t)}} (\boldsymbol{\omega}_{\mathrm{mesh}}\cdot\hat{\mathbf{n}})c\ d\partial\boldsymbol{\Psi}_{\mathrm{Soil}(t)}, \tag{93}$$

405 where, $\boldsymbol{\omega}_{\mathrm{mesh}}$ is the velocity of the boundaries $\boldsymbol{\Psi}_{p_j}$. This requires us to adapt
406 equation (50) so that,

$$\hat{\mathbf{n}}\cdot(\phi_w\boldsymbol{\nabla}c) = -(\boldsymbol{\omega}_{\mathrm{mesh}}\cdot\hat{\mathbf{n}})c, \quad \mathbf{x}\in\boldsymbol{\Gamma}_j. \tag{94}$$

407 Equation (94) then satisfies the conservation law for moving boundaries.

408 Secondly, as $\boldsymbol{\Psi}_{p_j}$ grows and $\boldsymbol{\Psi}_S$ is deformed, this causes an advective move-
409 ment effect on c within $\boldsymbol{\Psi}_S$. This can be interpreted as the boundaries of the
410 tubers and $\boldsymbol{\Gamma}_j$ physically pushing the nutrients. Hence, we are required to add
411 a conservative advection term to equation (48) accounting for the individual
412 elements within the mesh moving, *i.e.*,

$$(\phi_w + b)\partial_t c + c\partial_t\phi_w = \boldsymbol{\nabla}\cdot(\phi_w\boldsymbol{\nabla}c - \boldsymbol{\omega}_{\mathrm{mesh}}c) - \overline{g}c, \quad \mathbf{x}\in\boldsymbol{\Psi}_{\mathrm{Soil}}. \tag{95}$$

413 This modified system of equations can then be successfully implemented to
414 model coupled nutrient movement and poroelastic deformation from growing
415 tubers.

416 3.2 Homogenised Equations

417 The geometry we impose the homogenised set of equations on can be seen
418 in Figure 3a. However, to solve the set of homogenised equations (87)−(90),
419 we are required to solve a series of cell problems, *i.e.*, equations (75)−(77),
420 to calculate the terms $||\boldsymbol{\Omega}_{\mathrm{Soil}}(r_0)||$ and $\mathfrak{D}_{\mathfrak{e}}(r_0)$ that paramterise equation (88)
421 and (89). Since the geometric properties of the domain $\boldsymbol{\Omega}$ are contained in
422 $||\boldsymbol{\Omega}_{\mathrm{Soil}}(r_0)||$ and $\mathfrak{D}_{\mathfrak{e}}(r_0)$, we solve the cell problem for a series of different
423 tuber radii to correspond with different levels of growth/displacement from the

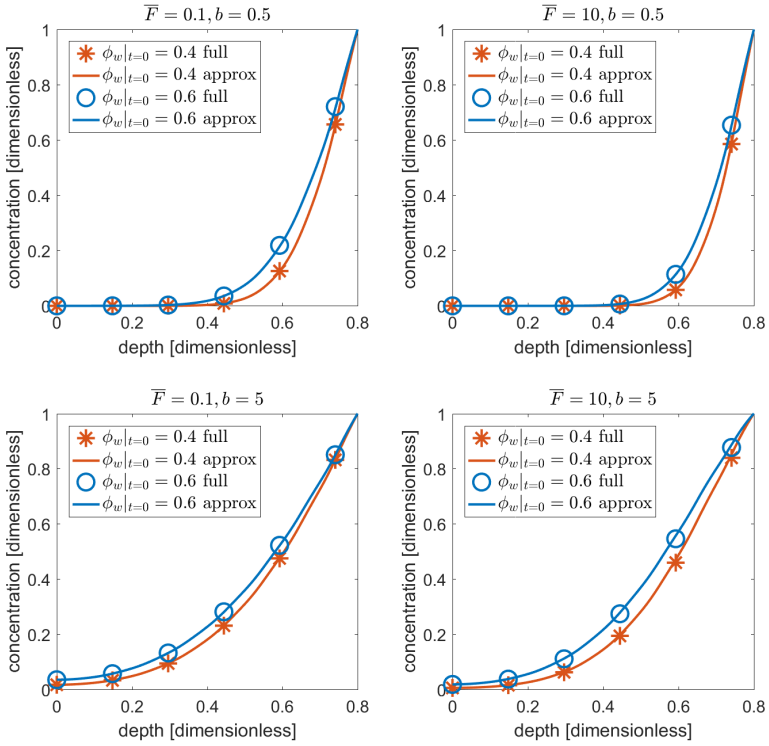

Fig. 4 Validation of homogenised equations (87)−(90) against the original set of equations (46)−(51). The plots show the nutrient profile c and c_0 from the base to the top of the domains shown in Figure 3 for a series of case studies using the parameter values $b \in \{0.5, 5\}$, $\overline{F} \in \{0.1, 10\}$, $\phi_w|_{t=0} \in \{0.4, 0.6\}$.

original tuber size. Using the results from the cell problems, we can construct interpolated functions to describe $||\boldsymbol{\Omega}_{\text{Soil}}(r_0)||$ and $\mathfrak{D}_{\mathfrak{e}}(r_0)$ as functions of the homogenised radius r_0.

3.3 Results

To validate the homogenisation procedure we compare the homogenised equations (87)−(90) against the original set of equations (46)−(51). We choose to run a series of case studies by varying the parameters b, $\overline{F}$ and $\phi_w|_{t=0}$. For the buffer power b we choose the values $b \in \{0.5, 5\}$ since this covers a range of buffer powers for the nutrients nitrogen, boron, magnesium, zinc and molybdenum [6]. From the non-dimensionalisation and parameter estimation we observe the value for root water uptake is $\overline{F} = \mathcal{O}(1)$. However to test the homogenisation procedure, we select the values $\overline{F} \in \{0.1, 10\}$ for low and high

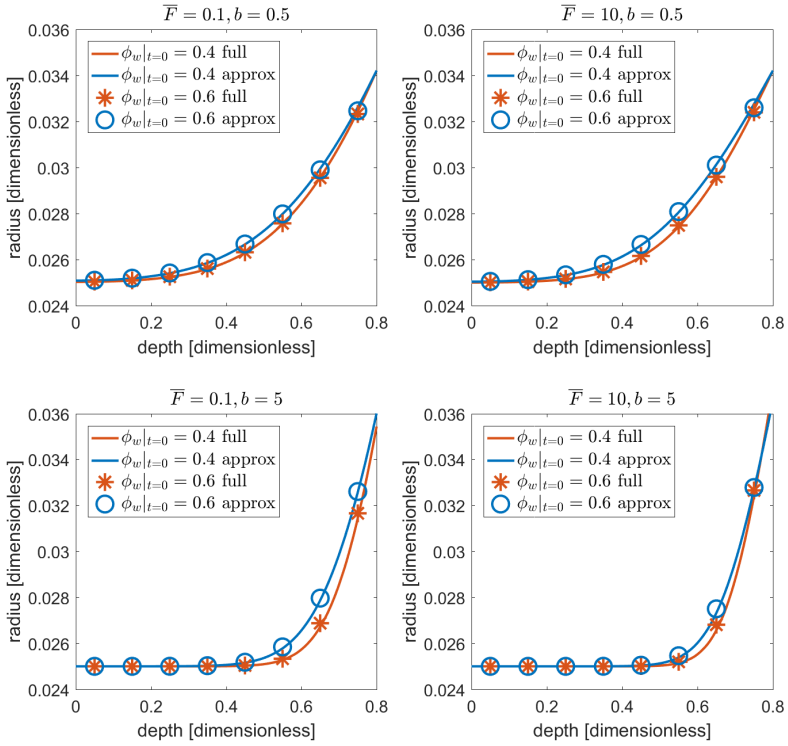

Fig. 5 Validation of homogenised equations (87)−(90) against the original set of equations (46)−(51). The plots show the effective radius r_0 against the actual radius r_j of the tubers from the base to the top of the domains shown in Figure 3 for a series of case studies using the parameter values $b \in \{0.5, 5\}$, $\overline{F} \in \{0.1, 10\}$, $\phi_w|_{t=0} \in \{0.4, 0.6\}$.

levels of water uptake respectively. Finally, for the initial water content $\phi_w|_{t=0}$ we assign the values $\phi_w|_{t=0} \in \{0.4, 0.6\}$ as these are approximate upper and lower bounds for silty soils [15].

In each of the simulations we impose a Dirichlet condition of $c = c_0 = 1$ on the top of each of the geometries shown in Figure 3a. Additionally, we choose the initial non-dimensionalised tuber radius to be $\overline{r^*} = 0.025$ and choose the remaining parameters to be $\overline{g} = \overline{\alpha} = 1$. We also impose a stop condition on each of the simulations so that when the non-dimensionalised volume of a tuber has doubled in magnitude, the simulation is terminated. Finally, in order to construct interpolated functions to describe $||\mathbf{\Omega}_{\text{Soil}}(r_0)||$ and $\mathfrak{D}_{\mathfrak{e}}(r_0)$ in equations (88) and (89), we solve a series of 6 cell problems with varying sphere radii.

Shown in Figure 4 are the nutrient profiles for c and c_0 down the length of the geometries shown in Figure 3a. We observe for all buffer powers, root uptake values and initial porosities, that the homogenised nutrient profile for

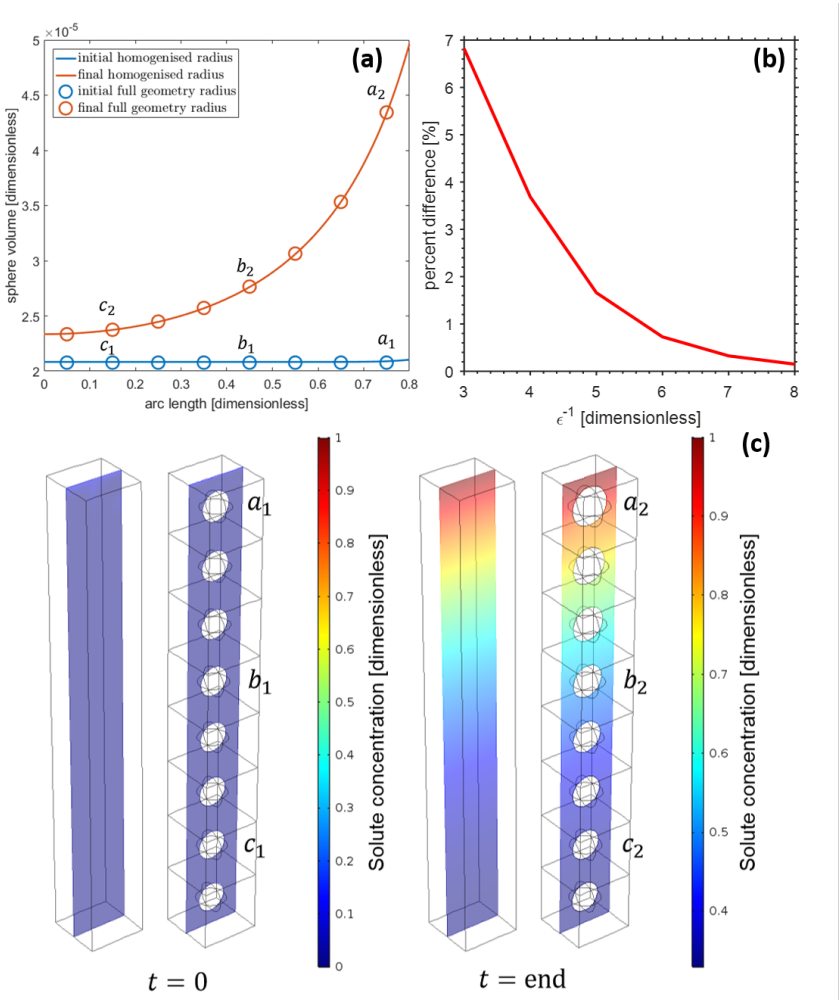

Fig. 6 (a): Shown are the results for the actual and effective tuber volumes for the simulation using the parameters $\overline{F} = 0.1, b = 0.5$ and $\phi_w|_{t=0} = 0.4$ at the beginning and end of the simulation.
(b): Illustrates the convergence of the full solution to the homogenised solution (presented as percent difference) as $\varepsilon \to 0$.
(c): Shown are the results for the actual and effective solute concentration for the same simulation as (a). Additionally the geometries capturing the tuber growth are shown.

c_0 is qualitively identical to the full nutrient concentration c. We find there to be a maximum error of $\lesssim 2\%$ between the solutions across all scenarios.

Additionally, shown in Figure 5 are the individual tuber radii r_j for the full set of equations against the effect radius r_0 from the homogenised equations. Similar to the results from Figure 4, we find that the effective radius r_0 successfully captures the growth of each tuber within the full domain shown in

Figure 3a. We find there to be a maximum error of $\lesssim 2\%$ between the actual and effective tuber radius.

To highlight the accuracy of the homogenised set of equations, shown in Figure 6 are detailed results for the simulation using the parameters $\overline{F} = 0.1$, $b = 0.5$ and $\phi_w|_{t=0} = 0.4$. From Figure 6a we observe that the effective radius r_0 is able to mimic the growth of the tubers in the full geometry. The growing tubers can be seen in Figure 6b, in which the tubers at the top of the full equation domain at the time point $t =$ end have grown substantially larger than those at the base of the domain. Furthermore, we find that the solute concentration profiles exhibit identical trains between the full and homogenised domains.

As a final confirmation of our model accuracy, we increased our mesh density from 21729 tetrahedral elements to 49218 elements in order to insure that our results are sufficiently accurate. Percent difference between the refined vs course solutions was on the order of 0.1%. This grants us confidence that our mesh is sufficiently resolved given the current problem. It is worth noting that our current simulations do not consider any automatic mesh refinement, as the deformations modelled do not result in any large aspect ratios. Under future considerations with more general geometries or greater deformations [16]. This would be more significant when considering large deformations, which are more common in soil materials [48].

From Figures 4 and 5, we observe that the homogenised equations successfully capture the nutrient movement and tuber growth in soil. However, the computation time between the two systems of equations differs by several orders of magnitude. We find that the full set of equations in three dimensions requires ≈ 5 minutes (300 seconds) to solve one simulation for eight periodic cells. Conversely, solving the homogenised equations requires ≈ 10 seconds to solve an analogous 3D simulation. Furthermore, the homogenised set of equations can be reduced to a 1D problem which will achieve the same results as the 3D problem due to the homogenisation procedure. We find that the computation time to solve the 1D problem is $\ll 1$ second, which is substantially faster than the full set of equations. However, a set of 3D cell problems is required to parameterise the homogenised set of equations for the terms $||\boldsymbol{\Omega}_{\text{Soil}}||$ and $\mathfrak{D}_{\mathfrak{e}}$. In this case study, we chose to conduct six cell problems for varying sphere radii. Each of the cell problems requires ≈ 10 seconds to solve. However, these cell problems are only required to be solved once for each set of parameters. Hence, we find that the homogenised sets of equations can reduce the computation time substantially whilst retaining a high level of accuracy. Furthermore, we can highlight the influence that the tubers' radii have on the effective homogenised diffusion coefficient (Figure 7). Under more dramatic growth scenarios where tubers increase their radii by a factor of 5, the effective diffusion in the system could be reduced by as much as 30%.

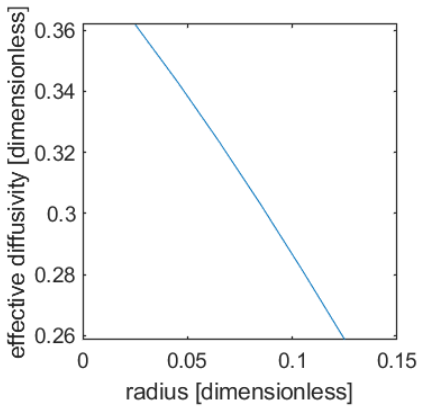

Fig. 7 Effective homogenised diffusivity coefficient as a function of potato radius.

4 Discussion

In this study, we developed a physical model for potato tuber growth that couples water and nutrient uptake with mechanical growth of potatoes in soil. The explicit consideration of the potato growth in the soil domain creates a physical impedance to nutrient transport through the soil. The geometry and the surface sinks due to the presence of potatoes impede the effective transport of nutrients through the soil domain (Figure 6). If impedance to diffusion caused by the potato tubers was not considered, we would incur an error between 175 to 300% in the effective diffusion of the solute (where the effective diffusion is $D_{eff} = \frac{\phi D}{\phi + b}$ in the case with no potatoes and $D^h_{eff} = \frac{\phi(r_0)\mathfrak{D}_\epsilon(r_0)}{(\phi(r_0)+b)||\mathbf{\Omega}_{\mathrm{Soil}(r_0)}||}$ when impedance to diffusion caused by growing tubers is homogenised). Furthermore, an error of up to 62.5% in effective diffusion could occur if the the tubers were modelled as a sphere with constant half of the final time dependent radius. These errors in effective diffusion would greatly impact the predicted solute leaching or plant solute uptake of models ignoring geometric impedance to diffusion.

One primary novelty associated with our growth model largely pertains to the growth domain locally external to our growing tubers. Similar studies have invoked a fluid-solid mechanical coupling to describe biological tissue as a porous medium, where cells are grow in an interstitial fluid [29,32]. These models deal with a saturated fluid domain interacting with a solid cell that is able to grow based on either nutrient uptake [29] or a prescribed growth rate [32]. Our model is applied to a partially saturated domain. Similar to [29], our biological agents grow proportional to the rate of nutrient uptake. However, our potato tubers also take up water, which impact the advective fluxes associated with the nutrient transport in the unsaturated soil domain.

As the focus of our system is to obtain a geometrically simplified model through our homoginisation procedure, the final equations that arise are convection-diffusion equations. By choosing a different re-scaling approach, it may be possible to obtain a similar Darcy type expression as demonstrated by [29] and [32], however, this was not within the scope of this study.

Previous studies have coupled fluid and solid mechanical systems to infer not only the impact that a solid inclusion would have on the fluid flow, but also the mechanical deformations that fluid flow would induce on the solid inclusion [38,9]. Authors have found that the homogenised system parameters are impacted by the distribution of inclusions in the domain. While our modelling scheme does not explicitly account for the mechanical response of the inclusions to externally applied stresses, the distribution of our potato tubers impact the flow and transport coefficients in a similar manner as demonstrated in previous studies [38]. It is worth noting that the growth behaviour of our modelled tubers implies a compensation for external stresses. Plant roots are known to respond to mechanical stresses by increasing their radii and reducing their length [1]. This behaviour does not readily lend itself to a simple coupling between mechanical stresses and growth responses, and future work should be conducted to better quantify these contrasting effects.

The full system of equations in this paper required the implementation of a complex moving boundary problem. This required the use of multiple domains to solve different components of the equations, and subsequent mappings of solutions across domains. Not only does this system require considerable computational power to solve, the time required to correctly implement this system is substantial. This is due to ensuring conservation of mass and consistent mappings of solutions across domains. Using mathematical homogenisation, many of the more cumbersome modelling aspects were simplified into an effective media, where the tuber surfaces are treated as domain sinks, and the tuber geometries are accounted for in the diffusivity term shown on Figures 4 and 5. Applying a similar method to a root system would facilitate a more rigorous quantification of bulk scale rhizosphere transport dynamics for both water and nutrients, generating better tools to disentangle the plant influence (rhizosphere soil) from the soil physical properties (bulk soil) [25].

Although the explicit model couples the poroelastic mechanical model to the transport equations for water and nutrients, a more specific mechanical coupling might be more appropriate to define the tubers expanding in partially saturated soil. Partially saturated soils are not subject to consolidation [48], thus considering the soil as an elasto-viscoplastic media may be important in this situation [19]. Furthermore, the mechanical stresses likely exceed typical yield stress values found in soil under field saturation conditions [20]. Previous models have utilised strictly linear-elastic parameters to quantify the mechanics of cavity expansion in unsaturated soil [3]; however, future work should attempt to remedy this by considering soil plasticity.

This study was motivated by the growth of tubers in soil, however, the system of equations is not limited to this particular problem. Other biological processes could also be modelled, including, but not limited too, clusters of

lymph nodes swelling under an inflammatory response from a disease or virus moving through a biological tissue [47], the growth of roots in response to water and nutrients [3,17], or to model the effect of tumour growth on nutrient flow during angiogenesis [2].

Technical analysis regarding the homogenisation procedure showed encouraging results. Comparing the results from the homogenised sets of equations to the full set yielded less than about a 2% difference between nutrient concentrations at different depths, Figure 4. Despite similarity in the results, the homogenised set of equations could be solved three orders of magnitude faster than the full set of equations, and, while the homogenised set of equations could readily be scaled with minimal increases to the computational time; increasing the domain size for the explicit geometry would increase the computational time substantially. This is important if we were to do combinatorial simulations spanning large numbers of soil and climate parameters to predict how potato crops grow. Thus, the averaged model will computationally allow extensive explorations of soil management and crop breeding strategies to be investigated *in silico*.

Acknowledgements SJD acknowledges a receipt of BBSRC Syngenta Case PhD studentship BB/L5502625/1. TR, KRD and DMMF are funded by ERC Consolidation grant 646809 DIMR. TR, and SR are funded by BBSRC SARISA BB/L025620/1

References

1. Abdalla, A., Hettiaratchi, D., Reece, A.: The mechanics of root growth in granular media. Journal of Agricultural Engineering Research **14**(3), 236–248 (1969)
2. Alarcón, T., Byrne, H.M., Maini, P.K.: A cellular automaton model for tumour growth in inhomogeneous environment. Journal of theoretical biology **225**(2), 257–274 (2003)
3. Aravena, J.E., Berli, M., Ruiz, S., Suárez, F., Ghezzehei, T.A., Tyler, S.W.: Quantifying coupled deformation and water flow in the rhizosphere using x-ray microtomography and numerical simulations. Plant and Soil **376**(1-2), 95–110 (2014)
4. Arbogast, T., Douglas Jr, J., Hornung, U.: Derivation of the double porosity model of single phase flow via homogenization theory. SIAM Journal on Mathematical Analysis **21**(4), 823–836 (1990)
5. Asfary, A., Wild, A., Harris, P.: Growth, mineral nutrition and water use by potato crops. The Journal of Agricultural Science **100**(1), 87–101 (1983)
6. Barber, S.A.: Soil nutrient bioavailability: a mechanistic approach. John Wiley & Sons (1995)
7. Bruna, M., Chapman, S.J.: Diffusion in spatially varying porous media. SIAM Journal on Applied Mathematics **75**(4), 1648–1674 (2015)
8. Cardaliaguet, P., Lions, P.L., Souganidis, P.: A discussion about the homogenization of moving interfaces. Journal de mathématiques pures et appliquées **91**(4), 339–363 (2009)
9. Chen, M., Kimpton, L., Whiteley, J., Castilho, M., Malda, J., Please, C., Waters, S., Byrne, H.: Multiscale modelling and homogenisation of fibre-reinforced hydrogels for tissue engineering. European Journal of Applied Mathematics pp. 1–29 (2019)
10. Comas, L., Becker, S., Cruz, V.M.V., Byrne, P.F., Dierig, D.A.: Root traits contributing to plant productivity under drought. Frontiers in plant science **4**, 442 (2013)
11. Daly, K., Cooper, L., Koebernick, N., Evaristo, J., Keyes, S., Van Veelen, A., Roose, T.: Modelling water dynamics in the rhizosphere. Rhizosphere (2017)
12. Daly, K., Roose, T.: Determination of macro-scale soil properties from pore-scale structures: model derivation. In: Proc. R. Soc. A, vol. 474, p. 20170141. The Royal Society (2018)

13. Daly, K.R., Roose, T.: Homogenization of two fluid flow in porous media. In: Proc. R. Soc. A, vol. 471, p. 20140564. The Royal Society (2015)
14. Darrah, P., Jones, D., Kirk, G., Roose, T.: Modelling the rhizosphere: a review of methods for 'upscaling' to the whole-plant scale. European Journal of Soil Science **57**(1), 13–25 (2006)
15. Das, B.M.: Advanced soil mechanics. Crc Press (2013)
16. Dehghani, H., Penta, R., Merodio, J.: The role of porosity and solid matrix compressibility on the mechanical behavior of poroelastic tissues. Materials Research Express **6**(3), 035,404 (2018)
17. Drew, M., Saker, L.: Nutrient supply and the growth of the seminal root system in barley: Iii. compensatory increases in growth of lateral roots, and in rates of phosphate uptake, in response to a localized supply of phosphate. Journal of Experimental Botany **29**(2), 435–451 (1978)
18. Essien, U., Akankpo, A., Igboekwe, M.: Poisson's ratio of surface soils and shallow sediments determined from seismic compressional and shear wave velocities. International Journal of Geosciences **5**(12), 1540 (2014)
19. Ghezzehei, T.A., Or, D.: Dynamics of soil aggregate coalescence governed by capillary and rheological processes. Water Resources Research **36**(2), 367–379 (2000)
20. Ghezzehei, T.A., Or, D.: Rheological properties of wet soils and clays under steady and oscillatory stresses. Soil Science Society of America Journal **65**(3), 624–637 (2001)
21. Godfray, H.C.J., Beddington, J.R., Crute, I.R., Haddad, L., Lawrence, D., Muir, J.F., Pretty, J., Robinson, S., Thomas, S.M., Toulmin, C.: Food security: the challenge of feeding 9 billion people. science **327**(5967), 812–818 (2010)
22. Hopmans, J.W., Nielsen, D.R., Bristow, K.L.: How useful are small-scale soil hydraulic property measurements for large-scale vadose zone modeling? Environmental Mechanics: Water, Mass and Energy Transfer in the Biosphere: The Philip Volume pp. 247–258 (2002)
23. Hornung, U.: Homogenization and porous media, vol. 6. Springer Science & Business Media (2012)
24. Keller, J.B.: Darcy's law for flow in porous media and the two-space method. Nonlinear partial differential equations in engineering and applied sciences **31**, 429–443 (1980)
25. Koebernick, N., Daly, K.R., Keyes, S.D., George, T.S., Brown, L.K., Raffan, A., Cooper, L.J., Naveed, M., Bengough, A.G., Sinclair, I., et al.: High-resolution synchrotron imaging shows that root hairs influence rhizosphere soil structure formation. New Phytologist **216**(1), 124–135 (2017)
26. Lesczynski, D., Tanner, C.: Seasonal variation of root distribution of irrigated, field-grown russet burbank potato. American Potato Journal **53**(2), 69–78 (1976)
27. Lions, P.L., Souganidis, P.E.: Homogenization of degenerate second-order pde in periodic and almost periodic environments and applications. In: Annales de l'Institut Henri Poincare (C) Non Linear Analysis, vol. 22, pp. 667–677. Elsevier (2005)
28. Nye, P.H., Tinker, P.B.: Solute movement in the soil-root system, vol. 4. Univ of California Press (1977)
29. O'Dea, R.D., Nelson, M., El Haj, A., Waters, S.L., Byrne, H.M.: A multiscale analysis of nutrient transport and biological tissue growth in vitro. Mathematical medicine and biology: a journal of the IMA **32**(3), 345–366 (2015)
30. Parker, C., Carr, M., Jarvis, N., Evans, M., Lee, V.: Effects of subsoil loosening and irrigation on soil physical properties, root distribution and water uptake of potatoes (solanum tuberosum). Soil and tillage research **13**(3), 267–285 (1989)
31. Pavliotis, G., Stuart, A.: Multiscale methods: averaging and homogenization. Springer Science & Business Media (2008)
32. Penta, R., Ambrosi, D., Shipley, R.: Effective governing equations for poroelastic growing media. Quarterly Journal of Mechanics and Applied Mathematics **67**(1), 69–91 (2014)
33. Rayleigh, L.: Lvi. on the influence of obstacles arranged in rectangular order upon the properties of a medium. The London, Edinburgh, and Dublin Philosophical Magazine and Journal of Science **34**(211), 481–502 (1892)
34. Roose, T., Fowler, A.: A mathematical model for water and nutrient uptake by plant root systems. Journal of theoretical biology **228**(2), 173–184 (2004)

35. Roose, T., Fowler, A.: A model for water uptake by plant roots. Journal of Theoretical Biology **228**(2), 155–171 (2004)
36. Roose, T., Fowler, A., Darrah, P.: A mathematical model of plant nutrient uptake. Journal of mathematical biology **42**(4), 347–360 (2001)
37. Roose, T., Keyes, S., Daly, K., Carminati, A., Otten, W., Vetterlein, D., Peth, S.: Challenges in imaging and predictive modeling of rhizosphere processes. Plant and Soil **407**(1-2), 9–38 (2016)
38. Royer, P., Recho, P., Verdier, C.: On the quasi-static effective behaviour of poroelastic media containing elastic inclusions. Mechanics Research Communications **96**, 19–23 (2019)
39. Sattelmacher, B., Klotz, F., Marschner, H.: Influence of the nitrogen level on root growth and morphology of two potato varieties differing in nitrogen acquisition. Plant and soil **123**(2), 131–137 (1990)
40. Sharma, M.: Wave propagation in a general anisotropic poroelastic medium: Biot's theories and homogenisation theory. Journal of Earth System Science **116**(4), 357 (2007)
41. Shock, C., Feibert, E., Saunders, L.: Potato yield and quality response to deficit irrigation. HortScience **33**(4), 655–659 (1998)
42. Van Genuchten, M.T.: A closed-form equation for predicting the hydraulic conductivity of unsaturated soils 1. Soil science society of America journal **44**(5), 892–898 (1980)
43. Vardanega, P., Bolton, M.: Stiffness of clays and silts: Normalizing shear modulus and shear strain. Journal of Geotechnical and Geoenvironmental Engineering **139**(9), 1575–1589 (2013)
44. Vereecken, H., Schnepf, A., Hopmans, J.W., Javaux, M., Or, D., Roose, T., Vanderborght, J., Young, M., Amelung, W., Aitkenhead, M., et al.: Modeling soil processes: Review, key challenges, and new perspectives. Vadose Zone Journal **15**(5) (2016)
45. Wang, H.F.: Theory of linear poroelasticity (2000)
46. Xu, X., Vreugdenhil, D., Lammeren, A.A.v.: Cell division and cell enlargement during potato tuber formation. Journal of Experimental Botany **49**(320), 573–582 (1998)
47. Yang, C.Y., Vogt, T.K., Favre, S., Scarpellino, L., Huang, H.Y., Tacchini-Cottier, F., Luther, S.A.: Trapping of naive lymphocytes triggers rapid growth and remodeling of the fibroblast network in reactive murine lymph nodes. Proceedings of the National Academy of Sciences **111**(1), E109–E118 (2014)
48. Yu, H.S.: Cavity expansion methods in geomechanics. Springer (2000)